Molecular Biology of the Cell
Vol. 21, 1556–1568, May 1, 2010

# Yip1A Structures the Mammalian Endoplasmic Reticulum

**Kaitlyn M. Dykstra, Jacqueline E. Pokusa, Joseph Suhan, and Tina H. Lee**

Department of Biological Sciences, Carnegie Mellon University, Pittsburgh, PA 15213

Submitted December 4, 2009; Revised March 2, 2010; Accepted March 8, 2010
Monitoring Editor: Benjamin S. Glick

**The structure of the endoplasmic reticulum (ER) undergoes highly regulated changes in specialized cell types. One frequently observed type of change is its reorganization into stacked and concentrically whorled membranes, but the underlying mechanisms and functional relevance for cargo export are unknown. Here, we identify Yip1A, a conserved membrane protein that cycles between the ER and early Golgi, as a key mediator of ER organization. Yip1A depletion led to restructuring of the network into multiple, micrometer-sized concentric whorls. Membrane stacking and whorl formation coincided with a marked slowing of coat protein (COP)II-mediated protein export. Furthermore, whorl formation driven by exogenous expression of an ER protein with no role in COPII function also delayed cargo export. Thus, the slowing of protein export induced by Yip1A depletion may be attributed to a proximal role for Yip1A in regulating ER network dispersal. The ER network dispersal function of Yip1A was blocked by alteration of a single conserved amino acid (E95K) in its N-terminal cytoplasmic domain. These results reveal a conserved Yip1A-mediated mechanism for ER membrane organization that may serve to regulate cargo exit from the organelle.**

## INTRODUCTION

The endoplasmic reticulum (ER) in most cell types is an interconnected membrane network of flattened sheet-like cisternae and narrow-diameter tubules dispersed throughout the cell cytoplasm (Baumann and Walz, 2001). The network is continuous with the outer nuclear envelope and extends outward toward the cell periphery. It is the largest membrane-bound organelle in animal cells and houses a wide array of essential cellular processes, including secretory and membrane protein biosynthesis and quality control, coat protein (COP)II-mediated secretory protein export, lipid synthesis, detoxification, and the regulation of intracellular $Ca^{+2}$ (Baumann and Walz, 2001).

To accommodate its varied functions, the ER is further subcompartmentalized into discrete subdomains (Baumann and Walz, 2001; Voeltz *et al*., 2002; Borgese *et al*., 2006; Shibata *et al*., 2006). Rough ER, enriched in membrane-bound ribosomes, is the primary site of protein biosynthesis and translocation, whereas smooth ER is the major site of $Ca^{+2}$ exchange, lipid synthesis, and detoxification. Between rough and smooth regions, the transitional ER comprises the subdomain where COPII vesicles bud to facilitate protein and lipid export. Each ER subdomain is generally thought to adopt the morphology most suited to its primary function. Thus, the flattened sheets of the rough ER may better accommodate large arrays of actively translating and translocating polysomes, whereas the greater surface-to-volume ratio associated with the highly curved tubules of the smooth ER may facilitate rapid transport of ions and lipids (Shibata *et al*., 2006).

In addition, the ER can adopt wide-ranging variations in structure and organization in specialized cell types (Borgese *et al*., 2006). Examples include the striking tubular morphology of the sarcoplasmic reticulum in muscle (Baumann and Walz, 2001; Rossi *et al*., 2008) and the dense parallel arrays of flattened rough ER sheets in the liver or pancreas (Rajasekaran *et al*., 1993; Baumann and Walz, 2001). The ER can also undergo dramatic expansion. For example, B lymphocytes undergo a severalfold increase in ER volume during differentiation (Wiest *et al*., 1990). Another type of frequently observed ER reorganization is the formation of tightly stacked membrane arrays of distinct architectures that yet retain continuity with the rest of the network (Chin *et al*., 1982; Yamamoto *et al*., 1996). These arrays can take on the appearance of compressed bodies of sinusoidal ER (Anderson *et al*., 1983), ordered arrays of tubules and sheets with hexagonal or cubic symmetry (Chin *et al*., 1982; Yamamoto *et al*., 1996), or concentric membrane whorls (Koning *et al*., 1996). Often, membrane packing or stacking occurs as a consequence of drug treatments (Jones and Fawcett, 1966; Hwang *et al*., 1974; Singer *et al*., 1988) or of up-regulation of a variety of membrane-anchored ER proteins such as cytochrome P450 (Koning *et al*., 1996), HMG-CoA reductase (Chin *et al*., 1982), microsomal aldehyde dehydrogenase (Yamamoto *et al*., 1996), cytochrome $b_5$ (Pedrazzini *et al*., 2000), or the inositol 1,4,5-triphosphate receptor (Takei *et al*., 1994). Significantly, tightly stacked and concentrically whorled ER membranes also have been observed in a large number of normal tissues (King *et al*., 1974), including testicular interstitial cells (Carr and Carr, 1962; Christensen and Fawcett, 1966), adrenocortical cells (Nickerson and Curtis, 1969), melanoma cells (Hu, 1971), cells of the anterior pituitary (Dubois and Girod, 1971), and hypothalamic arcuate neurons (King *et al*., 1974). In some instances, the whorled ER membranes are primarily smooth, but in others the whorled membranes also include ribosome-studded rough ER (King *et al*., 1974).

The prevalence of such large-scale ER reorganization is suggestive that form follows function. Indeed, ER membrane expansion in differentiating B lymphocytes increases the protein-folding capacity of the ER that enables massive up-regulation of antibody secretion (Wiest *et al*., 1990). The functional consequences of other types of ER reorganization, including concentrically whorled ER, is less well under-

This article was published online ahead of print in *MBoC in Press* (http://www.molbiolcell.org/cgi/doi/10.1091/mbc.E09–12–1002) on March 17, 2010.

Address correspondence to: Tina H. Lee (thl@andrew.cmu.edu).

stood. One possibility is that the tight packing of either smooth or rough membranes provides a means of sequestration and storage of either lipid or protein cargo for later use. Of note, many of the specialized cell types that have been observed to undergo ER stacking have roles in either peptide or steroid hormone secretion (King *et al*., 1974). In gonadotropin-releasing hormone (GnRH)-secreting hypothalamic arcuate neurons, the formation of ER whorls seems to also be regulated by the estrous cycle (King *et al*., 1974). Thus, large-scale ER reorganization may serve as a mechanism for regulating lipid or protein export in response to physiological cues.

Here, we identify a novel ER-structuring role for Yip1A, the mammalian homologue of a yeast protein implicated previously in the biogenesis of COPII transport vesicles from the ER (Heidtman *et al*., 2003). In its absence, the ER network is reorganized into concentrically whorled, stacked membranes. Stacked whorl formation is in turn sufficient to delay COPII-mediated ER export, consistent with the idea that whorled ER formation provides a means of delaying lipid or protein export. Together, our results suggest a role for Yip1A in the structural organization of the ER and raise the possibility that reorganization of ER membranes into whorls under certain physiological conditions may provide a means of transiently down-regulating cargo exit without directly modifying components of the COPII machinery.

## MATERIALS AND METHODS

### *Cell Culture, Constructs, and Transfections*

HeLa cells were maintained in minimal essential medium (Sigma-Aldrich, St. Louis, MO) containing 10% fetal bovine serum (Atlanta Biologicals, Norcross, GA) and 100 IU/ml penicillin and streptomycin (Mediatech, Herndon, VA) at 37°C in a 5% $CO_2$ incubator. Knockdown of HeLa cells stably expressing GalNacT2-green fluorescent protein (GFP) (Storrie *et al*., 1998) was performed with Oligofectamine (Invitrogen, Carlsbad, CA) as described previously, using 40 nM small interfering RNA (siRNA) (Kapetanovich *et al*., 2005), with the exception that a single transfection was sufficient for knockdown. The siRNAs were synthesized using the siRNA construction kit from Ambion (Austin, TX). The two siRNAs (−1, −2) used against Yip1A were made against the following target sequences, respectively: AAGTTACAGCATCGATGATCA and AATGGTTTTTTGCCTTGCTTT. The siRNA target sequence for Sar1a was AACCACTCTTCTTCACATGCT and AAGAACTGACCATTGCTGGCA for Sar1b. The control siRNA used throughout this study targeted bovine p115 and does not affect p115 in HeLa cells as described previously (Puthenveedu and Linstedt, 2004).

Transient cotransfection of HeLa cells with both plasmid DNA and siRNA was performed with Lipofectamine 2000 (Invitrogen) according to manufacturer's specifications by using 150 ng of DNA and 10 pmol of siRNA per 0.5 ml. Yip1A was cloned out of a HeLa cDNA library using polymerase chain reaction (PCR) and inserted into the pCS2-MT vector by using the EcoRI and XbaI sites. The FLAG-tagged Yip1A construct was generated by cutting out the myc-epitope using the BamHI and EcoRI sites, followed by the addition of a single FLAG epitope by using a PCR-based loop-in modification of the QuikChange protocol (Stratagene, La Jolla, CA). The Yip1A rescue construct was generated by introducing silent mutations into the siRNA-2 target sequence using QuikChange (AATGGTCTTCTGTCTTGCTTT). The E95K mutation in the rescue construct was also generated by QuikChange using the sequence GAGCCACCTTTATTAGAAAAGTTAGGTATCAATTTTGACCAC. The Myc-tagged Sec13 control construct was cloned by PCR amplification from HeLa cDNA and inserting the PCR product into the pCS2-MT vector by using BamHI and ClaI. The Myc-ts045 vesicular stomatitis virus glycoprotein (VSV-G) construct was cloned using PCR to amplify ts045 VSV-G and inserting the product into the pCS2-MT vector at the BamHI site. Myc-tagged DP1 and DP1L1 were generated by PCR amplification from HeLa cDNA and insertion into EcoRI and XbaI sites in pCS2-MT. Sec61γ-GFP (both monomeric [mGFP] and dimerizing [dGFP] forms) was kindly provided by Dr. E. Snapp (Albert Einstein University, Bronx, NY).

### *Antibodies and Other Reagents*

Antibodies used include mouse monoclonal antibody (mAb) against protein disulfide isomerase (PDI) (Abcam, Cambridge, MA); a rabbit polyclonal antibody (pAb) against Calnexin (Abcam); a rabbit pAb against BiP (Abcam); a rabbit pAb against LCB3 (Cell Signaling Technology, Danvers, MA); a rabbit pAb against tubulin (Abcam); rabbit pAbs against Giantin, GM130, and GRASP65 (kindly provided by Dr. A. Linstedt, Carnegie Mellon University, Pittsburgh, PA); a mouse mAb against ER-to-Golgi intermediate compartment (ERGIC)-53 (kindly provided by Dr. H.-P. Hauri, Biozentrum, University of Basel, Basel, Switzerland), the M2 mouse mAb against the FLAG epitope (Sigma-Aldrich); and a mouse mAb against the Myc epitope from the 9E10 cell line. Fluorophore-conjugated secondary antibodies were from Zymed Laboratories (South San Francisco, CA)/Invitrogen. A rabbit pAb was raised against a 6His-Yip1A (amino acids [aa] 1–89) fusion protein as antigen (Covance Research Products, Princeton, NJ) and was affinity purified on Affi-Gel 15 beads (Bio-Rad Laboratories, West Grove, PA) coupled with a glutathione transferase (GST)-Yip1A N-terminal fusion protein. A rabbit pAb was raised against GST-Sec13 (Covance Research Products) and affinity purified on Affi-Gel 10 beads (Bio-Rad Laboratories) coupled with 6His-Sec13. H89 was from Toronto Research Chemicals (North York, ON, Canada), and brefeldin A (BFA) was from Sigma-Aldrich.

### *Immunofluorescence and Immunoblot Assays*

siRNA transfections were analyzed 48–72 h after transfection as indicated. Immunofluorescence procedures were as described previously (Kapetanovich *et al*., 2005), except that a 20-min ice-cold methanol fixation was substituted for paraformaldehyde. Immunoblotting using our affinity-purified Yip1A antibody, as well as rabbit pAbs against calnexin and tubulin (Abcam), was performed on siRNA-treated cells harvested from 60-mm dishes as described previously (Kapetanovich *et al*., 2005).

### *Light Microscopy and Photobleaching Experiments*

All static images with the exception of those in Figure 4 were obtained using a Yokagawa spinning disk confocal scranhead (PerkinElmer Life and Analytical Sciences, Boston, MA) mounted on an Axiovert 200 microscope (Carl Zeiss, Jena, Germany) with a 100× 1.4 numerical aperture (NA) objective (Carl Zeiss) and acquired using a 12-bit Orca ER digital camera (Hamamatsu Photonics, Hamamatsu City, Japan). Maximal value projections of sections at 0.3-μm spacing (4-6/cell) were acquired using Imaging Suite software (PerkinElmer Life and Analytical Sciences). Quantitation of COPII assembly was carried out using ImageJ (National Institutes of Health, Bethesda, MD) as described previously (Kapetanovich *et al*., 2005). The wide field images in Figure 4 were obtained with a 63× 1.3 NA objective on an Axioplan microscope (Carl Zeiss) and acquired with QED software and a 12-bit Orca ER digital camera (Hamamatsu Photonics).

Fluorescence recovery after photobleaching (FRAP) analyses were performed on a 510 Meta/UV Duoscan Spectral Confocal with LSM Zen 2007 software by using a 100× 1.4 NA objective. Regions of interest were subjected to photobleaching with repeated pulses at 100% laser power with the pinhole wide open to obtain maximal depth of field. Recovery after photobleaching was monitored with attenuated laser power. To generate the fluorescence recovery curves, fluorescence within the photobleached region of interest at each time point was first normalized to that of a nonbleached reference region to account for general loss of fluorescence due to image acquisition. Recovery curves were then generated by setting the fluorescence intensity before bleaching to 100% and the intensity after the last bleach pulse to 0%.

### *Electron Microscopy*

Thirty-five-millimeter dishes of HeLa cells treated with control and Yip1A siRNA were fixed 48 or 72 h after transfection with 2% glutaraldehyde/phosphate-buffered saline (PBS) for 30 min at room temperature. After three washes in PBS, cells were further fixed in 2% potassium permanganate/$H_2O$ for 45 min, washed three times in distilled $H_2O$, followed by dehydration in an ascending series of ethanol (10–100%). Samples were then infiltrated in a 1:1 mixture of Epon-Araldite and 100% ethanol. After 30 min, the mixture was exchanged with 100% Epon-Araldite and held in a desiccator for 60 h. Samples were then transferred for 24 h each at 30, 40, 50, and 60°C. Epoxy disks were removed from the dishes, and areas of the disk with cells were cut out and glued onto a blank embedding capsule with two-part epoxy. Thin (100-nm) sections were cut using a DDK diamond knife on a Reichert-Jung Ultracut E ultramicrotome (Leica Microsystems, Wetzlar, Germany) and stained with lead citrate for 2 min. The grids were viewed on an H-7100 transmission electron microscope (Hitachi High Technologies America, Pleasanton, CA) operating at 75 kV. Digital images were obtained using an AMT Advantage 10 charge-coupled device Camera System (Advanced Microscopy Techniques, Danvers, MA) and ImageJ (National Institutes of Health).

### *Coimmunoprecipitation Assay*

For the pull-down of DP1 and DP1L1 with endogenous Yip1A, a 10-cm plate of HeLa cells was transfected with either Myc-DP1 or Myc-DP1L1 by using $CaPO_4$. After 72 h, cells were washed with ice-cold PBS and then scraped and solubilized for 30 min at 4°C for in HKT lysis buffer (100 mM KCl, 1% Triton X-100, 20 mM KHEPES, pH 7.2, and protease inhibitors). The lysate was then passed five times through a 25-gauge needle and then centrifuged for 20 min at 14,000 × *g*. The lysates were then incubated with 5 μl of antibody (immunoglobulin [Ig]G or Yip1A) bound to 15 μl of protein A-Sepharose beads (GE Healthcare, Little Chalfont, Buckinghamshire, United Kingdom) that had

been washed in lysis buffer. After a 2-h incubation at 4°C, the beads were washed three times with lysis buffer. The beads were then boiled for 10 min in 50 μl of 2× reducing sample buffer and resolved on a 10% SDS gel. Immunoblotting was performed using anti-Myc antibodies.

For the pull-down of DP1 using the FLAG-Yip1A constructs, 2 × 10-cm plates of HeLa cells were transfected with either Myc-DP1 only, FLAG-Yip1A-wt and Myc-DP1, or FLAG-Yip1A-E95K and Myc-DP1 by using jetPEI (Polyplus-Transfection, New York, NY) according to manufacturer's specifications. The immunoprecipitation was performed as described above; however, the lysates were incubated with anti-FLAG M2 agarose beads (Sigma-Aldrich).

### *ts045-VSV-G Transport Assay*

To assay ER export in Yip1A knockdown cells, HeLa cells were cotransfected with either Myc-ts045 VSV-G and a control siRNA, or Myc-ts045 VSV-G and Yip1A siRNA by using Lipofectamine 2000 (Invitrogen). Forty-eight hours after transfection, cells were placed at 40°C, the nonpermissive temperature for ER export of ts045 VSVG, to accumulate VSVG in the ER. After a 24-h incubation at the nonpermissive temperature, cells were shifted to the permissive temperature of 32°C for varying times. To assay ER export in cells expressing GFP-Sec61γ, HeLa cells were cotransfected with Myc-ts045 VSV-G and either dGFP-Sec61γ or mGFP-Sec61γ. Twenty-four hours after transfection, cells were shifted to 40°C and processed for the trafficking assay as described just above.

### *In Vitro COPII Assembly Assay in Yip1A Knockdown Cells*

Cells in a 10-cm dish were transfected with either control or Yip1A siRNA by using Oligofectamine (Invitrogen) and passaged onto coverslips after 24 h. After an additional 24 h, a second siRNA transfection was performed. Knockdown was monitored 48 h after the second transfection by immunostaining with Calnexin antibodies. At this time, the whorled ER phenotype was confirmed in >95% of cells. The COPII assembly assay was performed precisely as described previously (Lee and Linstedt, 2000) 72 h after the second transfection.

## RESULTS

### *Yip1A Knockdown Alters ER Network Organization*

Yip1 in yeast has been established as a cycling membrane protein required for COPII vesicle biogenesis (Heidtman *et al*., 2003). However, the mechanism by which it facilitates ER export remains largely unknown. There are two Yip1 isoforms in mammalian cells, Yip1A and Yip1B. Although each is 31% identical to yeast Yip1, Yip1B is expressed only in the heart, whereas Yip1A is ubiquitous (Tang *et al*., 2001). We therefore focused on Yip1A. Previous work suggests that both yeast Yip1 and mammalian Yip1A are ER-to-Golgi cycling proteins with a steady state pattern of localization coincident with ER exit sites and/or the ERGIC (Tang *et al*., 2001; Heidtman *et al*., 2003; Yoshida *et al*., 2008). Staining with our affinity-purified Yip1A antibodies confirmed a high degree of colocalization of Yip1A with ERGIC-53, a marker for the ERGIC (Supplemental Figure 1, A and B). Furthermore, consistent with the idea that Yip1A cycles constitutively through the ER and ERGIC compartments (Tang *et al*., 2001; Heidtman *et al*., 2003; Yoshida *et al*., 2008), blocking ER export using the protein kinase inhibitor H89 (Aridor and Balch, 2000; Lee and Linstedt, 2000), caused redistribution ($t_{1/2} \sim 10$ min) of Yip1A to the ER as observed previously (Lee and Linstedt, 2000) for the rapidly recycling ERGIC-53 (Supplemental Figure 1, C and D).

To determine the consequences of Yip1A depletion, Yip1A in HeLa cells was targeted for RNA interference (RNAi). Two different siRNAs targeting Yip1A yielded substantial knockdown of the protein as determined by immunoblot (Figure 1A). By indirect immunofluorescence, siRNA-1 and -2 both reduced Yip1A to near undetectable levels (compare Figure 1, D and F, to B), although a higher percentage of cells treated with siRNA-2 lacked detectable protein. To our initial surprise, cells lacking Yip1A displayed strikingly altered ER organization as marked by antibodies against the luminal ER resident PDI (Mazzarella *et al*., 1990). In contrast to control siRNA-treated cells with robust Yip1A staining (Figure 1B) and a typically dispersed tubular-reticular network that extended throughout the cell cytoplasm (Figure 1C), cells with undetectable Yip1A protein exhibited a notable loss of the peripheral tubular ER network and an apparent clustering of ER membranes into large micrometer-sized structures (Figure 1, E and G). The change in ER morphology was not marker specific. It was also readily observed with antibodies against the transmembrane ER resident calnexin (Ahluwalia *et al*., 1992). Moreover, the observed clustering of ER membranes seemed to reflect a reorganization of the ER as opposed to membrane proliferation, as shown by comparable levels of calnexin in control and Yip1A siRNA-treated cells (Figure 1A).

In addition to alterations in ER morphology, a marked fragmentation of the Golgi apparatus into mini-stacks was observed (Supplemental Figures 2, A–F, and 7), as reported previously (Yoshida *et al*., 2008). But despite extensive fragmentation of the Golgi, light level analysis revealed that Golgi marker separation was similar to that in control cells (unpublished data), and Golgi subcompartmentalization and its overall organization seemed to be maintained in cells lacking Yip1A (Supplemental Figure 7B). Several observations suggested that the striking ER rearrangements observed upon Yip1A knockdown were unlikely to have occurred as an indirect consequence of either Golgi fragmentation or redistribution of Golgi tethering and/or stacking proteins to the ER. First, a significant number of cells with clustered ER were detected as early as 48 h after Yip1A siRNA addition. At this time, ~50% of cells with clustered (or whorled; see below) ER showed as yet no noticeable Golgi fragmentation (Figure 1H). Second, the ER seemed normal in cells treated with siRNAs targeting either golgin160 (Yadav *et al*., 2009) or GRASP55 (Feinstein and Linstedt, 2008), even though the Golgi was fragmented in both cases (unpublished data). Third, both components of the Golgi tethering/stacking complex GM130/GRASP65 (Barr *et al*., 1997; Sengupta *et al*., 2009) colocalized with other Golgi markers in Yip1A-depleted cells (Supplemental Figure 2, G–L) in structures largely separate from the ER (Supplemental Figures 2, M–O, and 3). Finally, the ERGIC compartment was maintained mostly separate from the ER in cells lacking Yip1A, as evidenced by costaining with Yip1A and ERGIC-53 antibodies in control siRNA- and Yip1A siRNA-treated cells (Supplemental Figures 4 and 5).

### *Yip1A Loss Leads to ER Membrane Stacking*

Ultrastructural analysis by thin section electron microscopy (EM) corroborated the change in ER network organization seen at the light level. In contrast to control cells with a high density of ER membrane profiles in the cell periphery (Figure 2A), the majority of Yip1A knockdown cells were relatively devoid of identifiable peripheral ER membranes (Figure 2B). Instead, large densely packed membrane clusters were frequently observed (arrows in Figure 2B). Such densely packed ER structures were never observed in control cells. At higher magnification, the membrane clusters, clearly corresponding to the compacted ER membranes observed at the light level, were visible as stacked membranes arranged in concentric whorls ranging from 1 to 5 μm in outer diameter (Figure 2, C and D). The whorls were ER-derived because clear connections to the nuclear envelope were frequently observed (arrows in Figure 2, E and F). Connectivity of the whorls to the ER network was also demonstrated by relatively rapid diffusion of mGFP-sec61γ from the general ER into bleached whorls (Supplemental

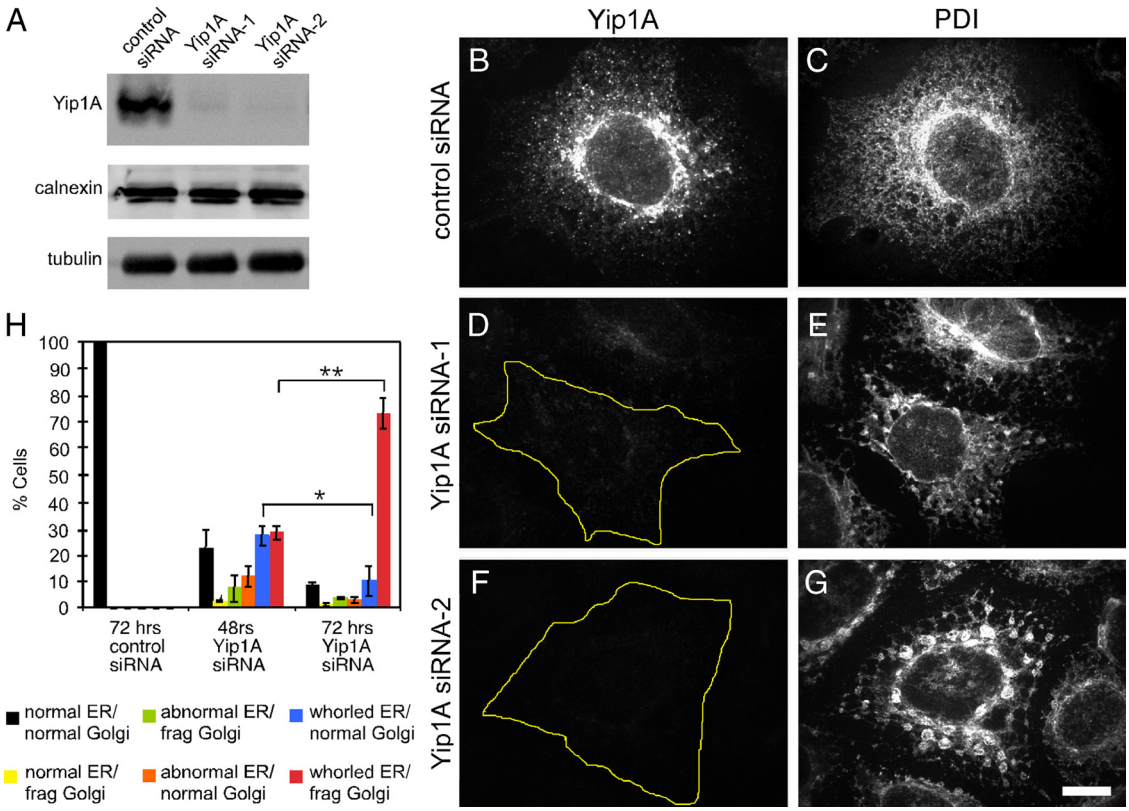


**Figure 1.** RNAi-mediated Yip1A depletion causes ER compaction. (A) Immunoblot demonstrating loss of Yip1A by two distinct siRNAs. HeLa cells stably expressing Golgi-localized GFP-GalNacT2 were transfected with a control siRNA, Yip1A siRNA-1, or Yip1A siRNA-2; harvested 72 h later; and probed using antibodies against Yip1A, calnexin, and tubulin. (B–G) Yip1A loss correlates with ER morphological changes. Cells transfected with control siRNA (B and C), Yip1A siRNA-1 (D and E), or Yip1A siRNA-2 (F and G) were fixed 72 h later and doubly stained with antibodies against Yip1A (B, D, and F) and PDI (C, E, and G). Bar, 10 $\mu$m. (H) ER morphological changes precede Golgi fragmentation. Cells transfected with a control siRNA or Yip1 siRNA-2 were fixed 48 or 72 h later and stained with antibodies against PDI. ER and Golgi morphologies were classified as indicated (frag Golgi, fragmented Golgi; whorled ER indicates compacted ER as shown in E and G; abnormal ER indicates ER morphologies intermediate between normal and whorled). Quantitation of the average percentage of cells displaying the indicated ER and Golgi morphologies from three independent experiments (>50 cells/condition/experiment) is shown, ±SD. Single asterisk indicates $p < 0.05$ and double asterisk indicates $p < 0.001$ (Student's *t* test).

Figure 6). Moreover, as expected for ER membranes, mitochondria were frequently in close apposition either to the whorls themselves or to membranes extending from the whorls. And, as suggested by light level analysis, Golgi cisternal organization seemed relatively normal in both control (Supplemental Figure 7A) and Yip1A knockdown cells (Supplemental Figure 7B), although the Golgi stacks were shorter in cells lacking Yip1A, as expected from the fragmentation seen at the light level.

Two observations suggested that the ER whorls were not a consequence of stress-induced ER autophagy. First, a limiting membrane (Bernales *et al*., 2006; Ogata *et al*., 2006) was never observed to surround the whorls. Second, immunoblotting with an antibody against BiP (Munro and Pelham, 1986), an ER chaperone that is up-regulated by ER stress (Ron and Walter, 2007), showed no increase in BiP protein expression (unpublished data). Third, immunostaining with antibodies against LCB3, a marker of autophagy (Kabeya *et al*., 2000), showed no change in knockdown cells (unpublished data). Finally, the tubulin-staining pattern in cells lacking Yip1A was indistinguishable from that in control cells (Supplemental Figure 8), rendering it unlikely that the effect of Yip1A depletion on ER organization was an indirect consequence of perturbation of the microtubule (MT) cytoskeleton (Terasaki *et al*., 1986).

Serial thin sections prepared from cells relatively early after knockdown (48 h) revealed that newly forming ER whorls were probably comprised of flat, sheet-like cisternae, as well as narrow-diameter tubules. In many whorls, concentric tubule-like arrays frequently persisted through multiple 100-nm serial sections, suggesting a structure made up predominantly of stacked sheets (Figure 3, A–I). However, newly forming whorls also contained membranes with more tubule-like morphology. For example, we observed whorls (Figure 3J) containing circular profiles that persisted for more than a single 100-nm section (Figure 3J, i and i′) as well as tubular profiles that did not persist for more than a single 100-nm section (Figure 3J, ii and ii′ and iii and iii′). Both were indicative of a tubular morphology. Thus, it seemed that the ER generally, both flat sheets and curved tubules, was transformed into a stacked and concentrically whorled arrangement upon Yip1A loss.

### *A Conserved Residue in the Cytoplasmic Domain of Yip1A Is Required for the ER Structuring Function*

To ascertain that the large-scale reorganization of the ER network into whorls was due specifically to Yip1A depletion, a siRNA-immune FLAG-Yip1A rescue construct was generated and cotransfected into cells along with the siRNA. Under these conditions, 66 ± 4% (3 independent experi-

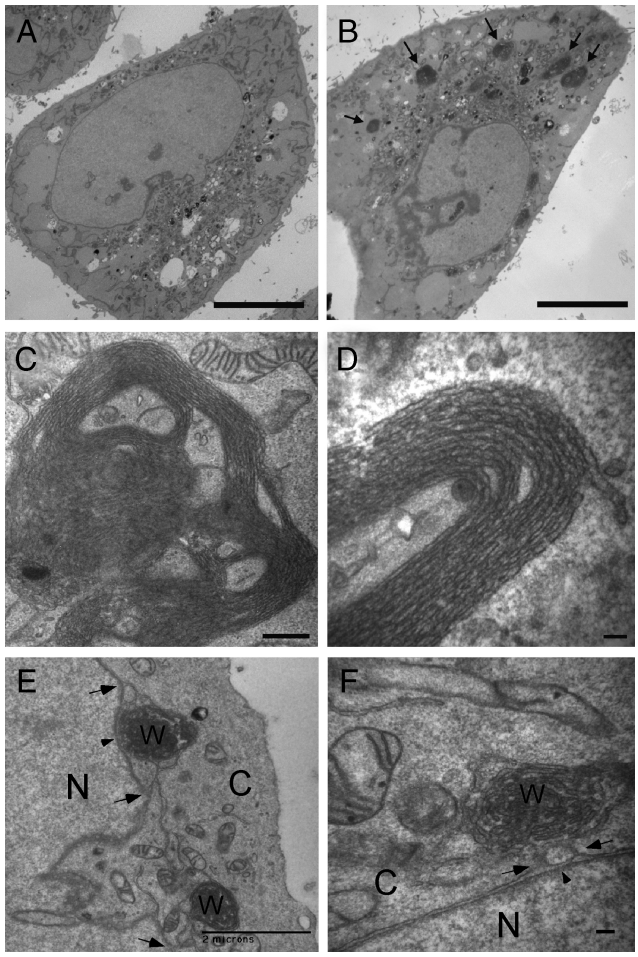


**Figure 2.** Ultrastructural analysis of cells lacking Yip1A. (A and B) A low-magnification thin section transmission EM view of cells treated with a control (A) or Yip1A (B) siRNA. Arrows (B) indicate dense ER membrane aggregates seen only in Yip1A siRNA-treated cells. Bar, 10 $\mu$m. (C) A higher magnification view of an entire ER whorl. Bar, 500 nm. (D) A high magnification view of stacked membranes of a portion of an ER whorl. Bar, 100 nm. (E and F) ER whorls are continuous with the nuclear envelope. A low-magnification view of two interconnected whorls each connected to the nuclear envelope (E) and a higher magnification view of a whorl exhibiting connections to the outer nuclear envelope (F). Arrowheads (E and F) indicate the nuclear envelope and arrows (E and F) indicate membrane continuities between whorl and nuclear envelope. N, nucleus; C, cytoplasm; W, whorl. Bar, 2 $\mu$m (E) and 100 nm (F).

ments of >50 cells/experiment) of cells expressing a control Sec13-Myc construct (Figure 4A) displayed the whorled ER phenotype (marked by single asterisks in Figure 4B, quantified in G). In contrast, virtually no cells expressing the FLAG-Yip1A rescue construct displayed whorled ER. That is, every cell expressing the FLAG-Yip1A rescue construct (Figure 4C) exhibited a normal dispersed, tubular-reticular ER network morphology (marked by double asterisk in Figure 4D, quantified in G). This result confirmed that the large-scale reorganization of the ER network observed upon treatment with Yip1A siRNA was indeed a specific consequence of Yip1A loss.

To determine whether the ER structuring function of Yip1A might depend on conserved and essential residues, we took advantage of a previously published mutagenesis study of yeast Yip1 wherein charged Yip1 residues conserved between yeast and mammals were individually altered and tested for effects on growth (Chen *et al*., 2004). Because a charge reversal of a specific Glu residue to Lys (E76K) in the N-terminal cytoplasmic domain of Yip1 rendered the protein nonfunctional for restoring growth even though the protein was stably expressed (Chen *et al*., 2004), we chose to test this version for its ability to structure the ER. Strikingly, 64 ± 1% of cells expressing FLAG-Yip1A (E95K) displayed the whorled ER phenotype despite the properly localized expression of protein (marked by single asterisks in Figure 4, E, F, quantified in G). Thus, the Yip1A (E95K) construct was no better than the negative control Sec13-Myc construct in its ability to rescue the whorled ER phenotype. This result indicates that the ER structuring function of Yip1A in mammals depends critically on a conserved, cytoplasmic residue.

### *Yip1A Interacts with the ER Structuring Protein DP1*

We reasoned that the inability of Yip1A (E95K) to fulfill its ER structuring function might stem from its inability to interact with a critical binding partner. Among the several Yip1 binding proteins identified in yeast (Matern *et al*., 2000; Calero *et al*., 2001; Chen *et al*., 2004; Heidtman *et al*., 2005), the ER integral membrane protein Yop1 stands out as a potential candidate for mediating the ER structuring function of Yip1. Deletion of Yop1 along with the structurally related Rtn1/Rtn2 in yeast resulted in a loss of cortical ER tubules (Voeltz *et al*., 2006); and purified Yop1 reconstituted into synthetic liposomes was sufficient to induce liposome tubulation (Hu *et al*., 2008). Furthermore, Yip1 overexpression in yeast suppressed lethality due to Yop1 overexpression, suggesting an antagonistic relationship between the two proteins (Calero *et al*., 2001). These observations prompted us to test whether DP1 (Voeltz *et al*., 2006), the mammalian homologue of Yop1, binds Yip1A. For this, Yip1A immunoprecipitation was performed on detergent-solubilized lysates from cells transfected with Myc-DP1. Indeed, both Myc-DP1 and the related Myc-DP1L1 (50% identical) were recovered on Yip1A antibody beads but not on control antibody beads (Figure 5A).

To next assess whether the inability of Yip1A (E95K) to structure the ER might be due to an inability to bind DP1, an antibody against the FLAG epitope tag was used to immunoprecipitate FLAG-Yip1A from cells cotransfected with Myc-DP1 and either wild-type FLAG-Yip1A or Flag-Yip1A (E95K). As shown (Figure 5B), Myc-DP1 was recovered in association with both the wild type and the E95K variant of FLAG-Yip1A. Therefore, the inability of Yip1A (E95K) to maintain a dispersed ER network cannot be attributed simply to its failure to bind the ER structuring protein DP1. Further work is required to elucidate the functional relevance of the Yip1A–DP1 interaction for ER structuring.

### *Yip1A Depletion Slows VSVG Export from the ER without Affecting COPII Recruitment*

Our results thus far indicated that Yip1A was required specifically to maintain a dispersed tubular-reticular ER network. Because previous studies in yeast had implicated Yip1 in COPII-mediated ER export, we next compared the kinetics of ts045 VSV-G ER export (Kreis and Lodish, 1986; Presley *et al*., 1997) in the presence and absence of Yip1A. For this, cells were cotransfected with either Myc-tagged ts045 VSV-G and a control siRNA, or Myc-ts045 VSV-G and Yip1A siRNA. Forty-eight hours after transfection, cells were placed at 40°C, the nonpermissive temperature for ER export of ts045 VSV-G, to accumulate VSV-G in the ER. After a 24-h incubation at the nonpermissive temperature, cells were shifted

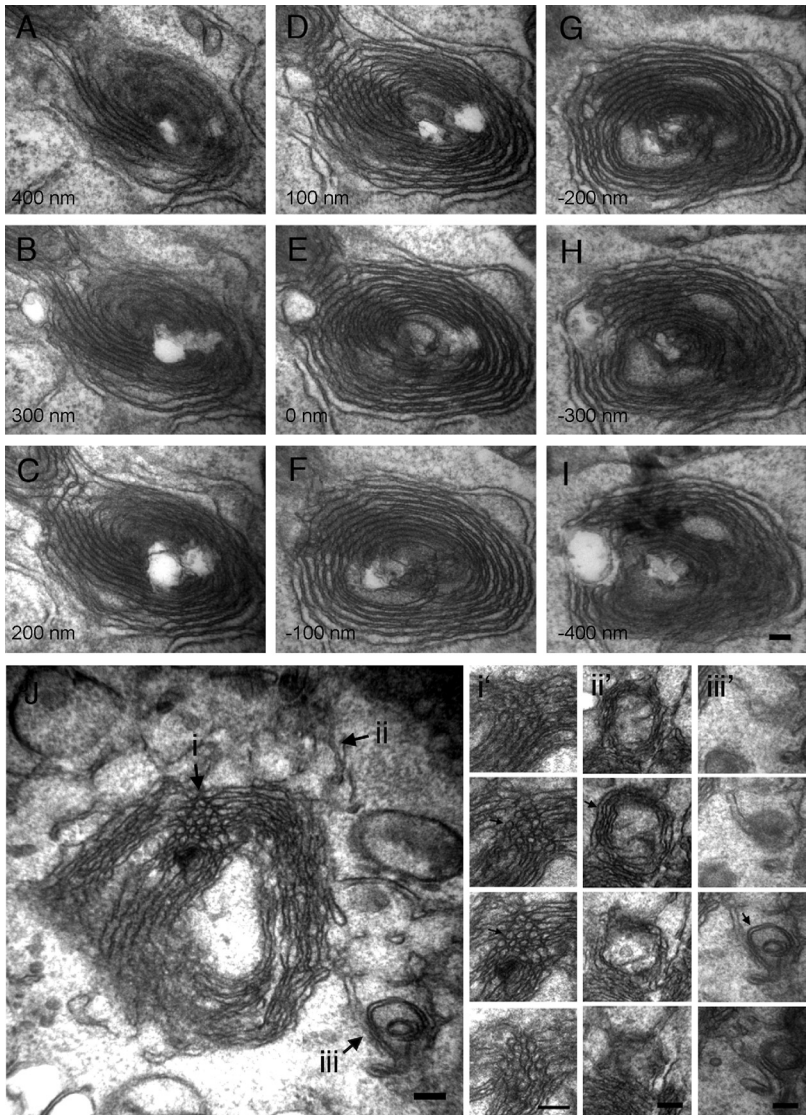


**Figure 3.** Early ER whorls consist of both sheets and tubules. (A–I) Serial (100-nm) transmission EM thin sections through an ER whorl 48 h after Yip1A siRNA treatment. Bar, 100 nm. (J) A thin section micrograph through a different ER whorl 48 h after Yip1A siRNA treatment. Arrows (i, ii, and iii) indicate three different examples of tubular morphology. Serial 100-nm thin sections through the corresponding regions (i, ii, and iii) of the whorl in J are shown in i', ii', and iii'.

to the permissive temperature of 32°C for 0, 20, 60, or 120 min. As expected, VSV-G moved synchronously from the ER (Figure 6A) to the Golgi (Figure 6B) by 20 min and to the surface (Figure 6C) by 60 min in control siRNA-treated cells (quantified in Figure 6G). In Yip1A knockdown cells, VSV-G also accumulated in the ER at the nonpermissive temperature (Figure 6D). Indeed, staining for Myc-VSV-G in these cells allowed ready visualization of the whorls induced by Yip1A loss. In contrast to the control cells, however, a significant fraction of Yip1A knockdown cells retained VSV-G in the ER at 20 min (Figure 6E). Cells lacking Yip1A function were identified by the presence of whorled ER structures after doubly staining with calnexin antibodies. By 20 min, VSV-G had moved out of the ER in only ~20% of cells displaying whorled ER membranes (Figure 6G). In the remaining 80% of Yip1A knockdown cells, VSV-G was clearly retained in whorled ER membranes (Figure 6E, quantified in G). By 60 min, the fraction of cells with VSV-G in whorled ER declined to ~30% and VSVG was detected in the Golgi and/or surface in ~70% of cells (quantified in Figure 6G). By 120 min, ER export of VSV-G had occurred in >80% of cells displaying whorled ER (Figure 6F, quantified in G). Thus, ER export was significantly delayed, though not altogether blocked, in the absence of Yip1A. The marked slowing of ER export upon loss of Yip1A function was in agreement with studies in yeast (Heidtman *et al*., 2003).

To determine whether the slowing of ER export might be due to defects in the recruitment and assembly of COPII subunits to ER exit sites, the steady state distribution of the COPII subunit Sec13 was examined in cells with and without Yip1A. For this, cells were cotransfected with Sec13-Myc and either a control siRNA or Yip1A siRNA. As expected, control cells exhibited a robust Sec13-Myc distribution consistent with an ER exit site pattern (Figure 7A). Assembled COPII structures were distributed throughout the dispersed ER (Figure 7B, merge in C). Surprisingly, Yip1A knockdown cells also exhibited a robust Sec13-Myc distribution (Figure 7D), even in cells with extensive ER whorling (Figure 7E). Notably, Sec13 positive structures seemed to be largely excluded from the whorled ER (arrows in merge in Figure 7F). This result suggested that Yip1A was not required for the recruitment of COPII subunits to presumptive ER exit sites, although the exit sites formed in its absence seemed altered in their distribution.

To further assess the ability of cells lacking Yip1A to recruit COPII proteins to the ER, an in vitro COPII assembly

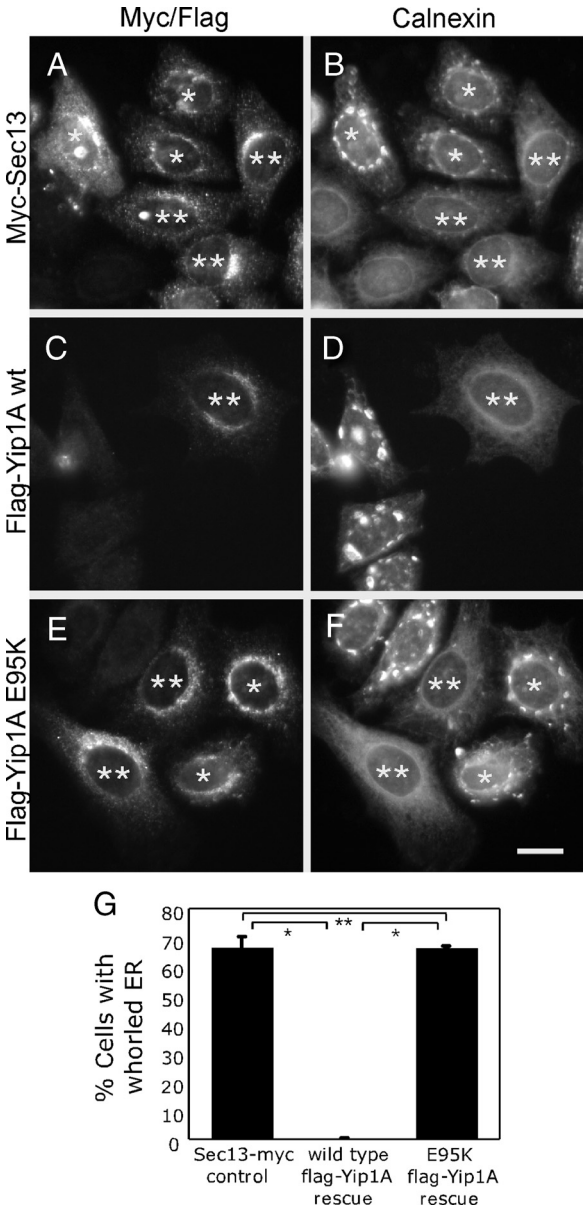


**Figure 4.** The whorled ER phenotype is rescued by a wild type but not mutant siRNA-immune Yip1A construct. Cells cotransfected with Yip1A siRNA-2 and either a control Sec13-Myc construct (A and B), a siRNA-immune wild-type FLAG-Yip1A construct (C and D), or a siRNA-immune mutant (E95K) FLAG-Yip1A construct (E and F) were fixed 72 h later and doubly stained with antibodies against the Myc epitope (A) and calnexin (B) or the FLAG epitope (C and E) and calnexin (D and F). Single asterisks (A–F) indicate expressing cells that exhibit ER whorls. Double asterisks (A–F) indicate expressing cells that do not exhibit ER whorls. Bar, 10 $\mu$m. (G) Quantitation of the percentage of Sec13-Myc or wild type or mutant (E95K) FLAG-Yip1A–expressing cells displaying the whorled ER phenotype from three independent experiments (>50 cells per experiment), ±SD. Single asterisks indicate $p < 0.0001$ (Student's *t* test). Double asterisk indicates no statistically significant difference.

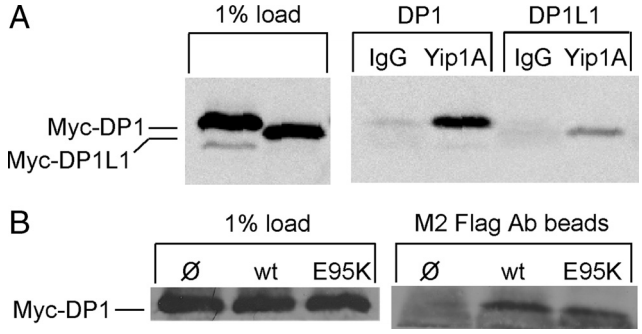


**Figure 5.** Both wild-type and E95K Yip1A bind to DP1. (A) HeLa cells transfected with either Myc-DP1 or Myc-DP1L1 were solubilized in 1% Triton X-100 and subjected to immunoprecipitation with either a control antibody (IgG) or Yip1A antibody. Bound protein was subjected to immunoblotting with an antibody against the Myc epitope. (B) HeLa cells cotransfected with Myc-DP1 and either wild-type FLAG-Yip1A or FLAG-Yip1A (E95K) were solubilized in 1% Triton X-100 and subjected to immunoprecipitation with M2 FLAG antibody beads. Bound protein was subjected to immunoblotting with the Myc epitope antibody. As a control, the Myc-DP1 recovered on M2 beads in the absence of FLAG-Yip1A is also shown.

assay was also performed. To ensure that most of the Yip1A siRNA-treated cells used in the assembly assay were depleted of Yip1A, a double sequential knockdown was performed. Then, to confirm efficient depletion, cells were stained with antibodies against calnexin 24 h before the assembly assay. At this time, >95% of the doubly transfected Yip1A knockdown cells displayed the whorled ER morphology, confirming efficient Yip1A depletion. To monitor the ability of the ER to support COPII assembly in the absence or near complete absence of Yip1A, cells were subsequently permeabilized with digitonin to extract endogenous COPII proteins (Kapetanovich *et al*., 2005). The permeabilized cells were then incubated in the presence or absence of rat liver cytosol. As expected, COPII assembly did not occur in the absence of added cytosol (Figure 7G) but was robust in the presence of added cytosol (Figure 7H) in control siRNA-treated cells. Also as expected, cells depleted of Yip1A were incapable of supporting COPII assembly in the absence of added cytosol (Figure 7I). However, assembly was again surprisingly robust in the presence of added cytosol (Figure 7J, quantified in K). Thus, although COPII-mediated ER export was significantly delayed in the absence of Yip1A, the delay seemed not to be a simple consequence of inhibition of coat protein recruitment to ER membranes.

### *Blocking ER Export Does Not Induce ER Stacking*

Two straightforward models could account for both the loss of normal ER network morphology and the slowing of ER export in response to Yip1A loss: 1) Yip1A is required primarily for COPII vesicle biogenesis but the inhibition of COPII function resulting from Yip1A loss secondarily cause changes in ER structure. 2) Yip1A is required primarily for ER morphogenesis, but the structural rearrangements resulting from Yip1A depletion secondarily inhibit COPII function. To distinguish between these models, we first asked whether an ER export delay similar to that caused by Yip1A loss, but induced by independent means, would lead to ER organizational changes such as those seen in Yip1A knockdown cells. ER export blockade was imposed by two independent means. In the first, cells were treated with siRNAs targeting both Sar1a and Sar1b (Kuge *et al*., 1994), a GTPase required for COPII assembly and vesicle formation (Nakano and Muramatsu, 1989). After confirming a block in ER export in Sar1a/b double knockdown cells (Figure 8A), ER morphology was assessed. As expected, the ER network in control cells with normal levels of assembled Sec13 (Figure

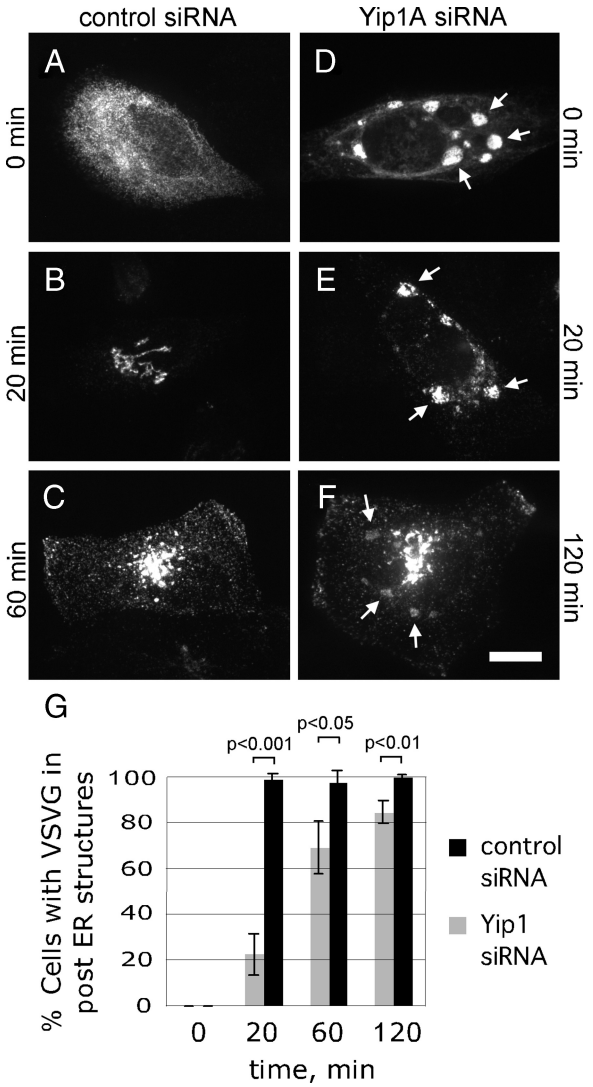


**Figure 6.** Export of ts045 VSV-G from the ER is slowed by ER whorling. (A–F) Cells cotransfected with Myc-ts045 VSV-G and either a control siRNA (A–C) or Yip1A siRNA-2 (D–F) were shifted 48 h after transfection to 40°C to accumulate VSV-G in the ER. After an additional 24 h, cells were shifted to 32°C for 0 (A and D), 20 (B and E), 60 (C), or 120 (F) min to allow ER export. Cells were fixed and doubly stained with antibodies against the Myc epitope and calnexin (only the Myc staining is shown). Arrows (D–F) indicate the positions of ER whorls as marked by Calnexin staining. Bar, 10 $\mu$m. (G) Quantitation of the percent of cells expressing Myc-ts045 VSV-G with the protein in post-ER structures. For cells transfected with Yip1A siRNA, only cells with whorled ER, as marked by Calnexin staining, were quantified. Shown are the averages from three independent experiments, ±SD (p values obtained using the Student's *t* test).

8B) was typically dispersed (Figure 8C). Significantly, cells with only background levels of assembled Sec13 (Figure 8D) also had a relatively normal dispersed ER network morphology (Figure 8E). Similar results were obtained when COPII assembly was blocked by another means, this time by treatment with the protein kinase inhibitor H89 (Aridor and Balch, 2000; Lee and Linstedt, 2000). Treatment of cells with H89 caused a rapid redistribution of ERGIC-53 from its typical ERGIC localization (Figure 8F) to an ER-like pattern (Figure 8H), indicating efficient ER export blockade by H89. Nonetheless, the morphology of the ER, as marked by PDI staining, was similar in both untreated (Figure 8G) and H89-treated (Figure 8I) cells. Thus, neither of two independent means of blocking ER export yielded an ER morphological resembling that obtained by Yip1A depletion. Therefore, the whorled ER phenotype observed upon Yip1A depletion was unlikely to have occurred as a secondary consequence of inhibiting ER export.

### *ER Stacking Is Sufficient to Slow ER Export*

We next considered the alternate model, that ER membrane stacking caused by Yip1A loss might be sufficient to delay ER export and account for the diminishment of COPII function in cells lacking Yip1 function. In support of this hypothesis, membrane stacking induced by an unrelated method has been shown previously to delay VSV-G export from the ER (Amarilio *et al*., 2005). In that case, overexpression of the integral ER membrane-anchored VAP-B/Nir2 complex was suggested to lead to membrane stacking through transdimerization of VAP-B/Nir2 complexes on opposing membranes, leading to a membrane zippering effect (Amarilio *et al*., 2005). One caveat, however, is that VAP-B, like Yip1A, also has been suggested to function in ER-to-Golgi trafficking (Soussan *et al*., 1999). Thus, it remained possible that the delay in ER export induced by VAP-B/Nir2 overexpression could be attributed to a direct role for VAP-B in ER-to-Golgi trafficking. To address this caveat, we sought a means of inducing ER stacking that was unlikely to impact ER export directly. For this, we took advantage of a previous study demonstrating that overexpression of a dimerizing GFP-Sec61$\gamma$ fusion protein (dGFP-Sec61$\gamma$) could drive ER stacking through head-to-head interactions between ER membrane-anchored GFP monomers on opposing ER membranes (Snapp *et al*., 2003). Because neither Sec61$\gamma$ nor GFP have any role in COPII function, we reasoned that this method of inducing ER membrane stacking provided a way of testing whether ER membrane stacking per se might be sufficient to delay ER export.

To assess ER export efficiency, the time course of VSV-G ER export in cells expressing dGFP-Sec61$\gamma$ was compared with that in cells expressing mGFP-Sec61$\gamma$, a variant incapable of inducing ER stacking due to a mutation in a residue required for GFP dimerization (Snapp *et al*., 2003). As anticipated, cells expressing dGFP-sec61$\gamma$ exhibited compacted ER structures (Figure 9, B, E, H, and K) shown previously to correspond to stacked and whorled ER membranes by EM (Snapp *et al*., 2003). Also, as anticipated, Myc-ts045 VSV-G was predominantly in the compacted ER structures before shift to the permissive temperature (Figure 9, A–C). Even 20 min after the shift, at a time when VSV-G had exited the ER in nearly all cells expressing the control mGFP-Sec61$\gamma$ construct (Figure 9M), nearly 80% of cells with compacted ER retained VSV-G in the compacted ER structures (Figure 9, D–F, quantified in M). Therefore, the export of VSV-G from the ER was slowed markedly by ER membrane stacking. Export was not blocked though, as VSV-G reached post-ER structures in ~50% of cells with stacked ER by 60 min (Figure 9, G–I and M), and the number increased further to ~70% at the 120-min time point (Figure 9, J–L and M). Interestingly, the kinetics with which VSV-G exited the ER in these cells mirrored closely the kinetics with which it exited the ER in Yip1A knockdown cells. The results support the notion that membrane stacking per se is sufficient to reduce ER export kinetics. Altogether, the results described herein suggest that Yip1A plays a novel ER network dispersal function. ER network dispersal by Yip1A in turn is required for rapid ER export.

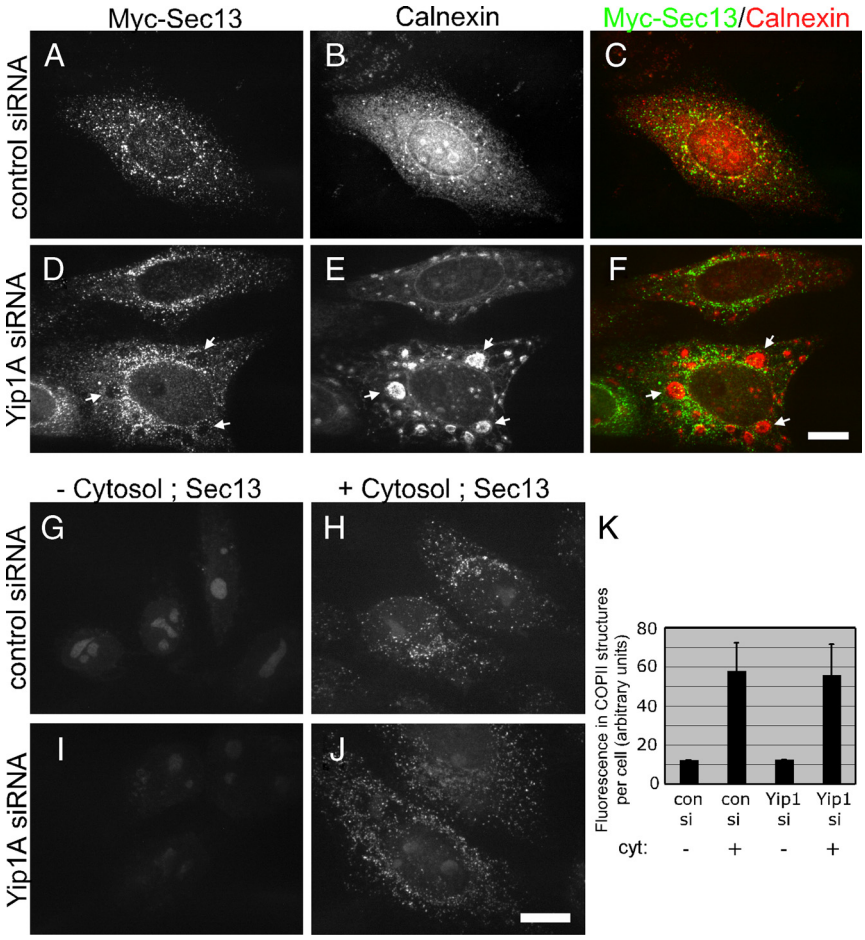


**Figure 7.** COPII recruitment is not blocked in cells lacking Yip1A. (A–F) Cells cotransfected with Sec13-Myc and either a control siRNA (A–C) or Yip1A siRNA-2 (D–F) were fixed 72 h later and doubly stained with antibodies against the Myc epitope (A and D) and calnexin (B and E). The merge is also shown (C and F). Arrows (D–F) indicate the lack of Sec13-Myc in ER whorls. Bar, 10 $\mu$m. (G–K) Cytosol dependent COPII assembly does not require Yip1A. Cells doubly transfected with a control (G and H) or Yip1A siRNA-2 (I and J) were permeabilized with 30 $\mu$g/ml digitonin 72 h after the second transfection and incubated with an ATP-regenerating system and guanosine 5′-*O*-(3-thio)triphosphate in the absence (G and I) or presence (H and J) of 4 mg/ml rat liver cytosol. After 20 min at 37°C, cells were fixed and stained with antibodies against Sec13. Bar, 10 $\mu$m. (K) Quantitation of the total fluorescence in Sec13-positive structures under the indicated conditions is shown, three independent experiments, ±SD.

## DISCUSSION

Yip1A depletion in mammalian cells led to dramatic alterations in ER network organization unlike any previously documented for a specific loss of function perturbation. Based on the combined data, we hypothesize that Yip1A plays a role in maintaining a dispersed ER network. In its absence, ER membranes undergo a stacking and whorl formation reaction that in turn slows protein export. Our results also provide experimental support for the notion that a general change in the organization of the ER network can significantly impact rates of protein export from the organelle. Furthermore, they suggest the possibility that certain specialized cells might use large-scale ER reorganization to elicit transient changes in the secretory capacity of the ER.

Previous studies have reported variable degrees of Golgi fragmentation but no ER morphological change or delay in ER-to-Golgi trafficking after Yip1A RNAi (Yoshida *et al.*, 2008; Kano *et al.*, 2009). A potential underlying explanation for the observed differences in the knockdown phenotype is the extent of Yip1A depletion obtained with distinct siRNAs. Indeed, we have observed a strong correlation between ER morphology and the level of residual Yip1A protein remaining after knockdown. Cells without detectable Yip1A almost always displayed the whorled ER phenotype, whereas cells with residual Yip1A did not, suggesting that low levels of Yip1A are able to maintain a relatively dispersed ER network.

### *The Basis for Inhibition of ER Export by ER Membrane Stacking and Whorling*

Why does ER membrane stacking and whorling delay COPII-mediated protein export? COPII proteins were recruited efficiently to presumptive ER exit sites even in the absence of Yip1A, and yet ER export of VSVG was markedly slowed. One potential explanation is that reorganization of a large fraction of the ER into stacked whorls sequesters cargo molecules away from cytoplasmic coat proteins, thereby reducing the efficiency of cargo capture by the COPII coat. Thus, COPII vesicle formation per se might proceed in the absence of Yip1A, but the resulting vesicles might contain reduced amounts of cargo. Although our FRAP data suggest that the diffusion of mGFP-Sec61$\gamma$ into and presumably out of whorls is relatively unrestricted (Supplemental Figure 6), the diffusional mobility of VSV-G has not yet been examined and may be preferentially hindered. An alternative possibility is that a late step in COPII vesicle biogenesis, subsequent to the initial steps of Sar1 activation and coat protein recruitment, is sensitive to the membrane morphological changes associated with ER stacking and whorling. Generation of either positive or negative membrane curvature or the mixing of phospholipids ultimately required for vesicle budding may comprise this late step.

### *Yip1A May Regulate the Ability of One or More ER Proteins to Interact In Trans*

Although the MT cytoskeleton and associated motor proteins are acknowledged to play a key role in extending ER

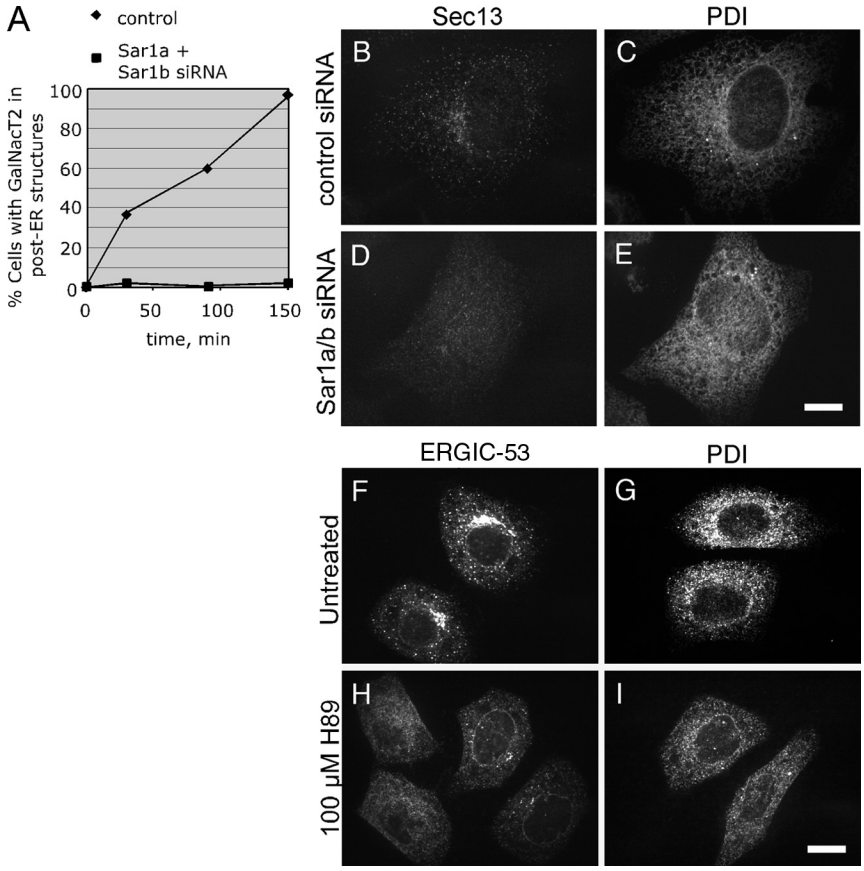


**Figure 8.** ER export blockade is not sufficient to cause ER whorling (A–E). (A) Sar1 knockdown blocks ER export. HeLa cells expressing the Golgi marker GFP-GalNacT2 and transfected with a control siRNA or siRNAs targeting both Sar1a and Sar1b isoforms were treated with 2.5 $\mu$g/ml BFA for 30 min to redistribute GFP-GalNacT2 to the ER and subsequently incubated without drug to allow ER export. At the indicated times, cells were fixed, and the percentage of cells with GFP-GalNacT2 in post-ER structures was counted. (B–E) ER export blockade by Sar1 knockdown does not affect ER morphology. Control (B and C) or Sar1 knockdown cells (D and E) were fixed 72 h after transfection and doubly stained with antibodies against Sec13 (B and D) and PDI (C and E). Bar, 10 $\mu$m. (F–I) ER export blockade by H89 treatment does not affect ER morphology. Untreated cells (F and G) or cells treated for 20 min with 100 $\mu$M H89 (H and I) were fixed and stained singly for ERGIC-53 (F and H) or PDI (G and I). Bar, 10 $\mu$m.

tubules toward the cell periphery (Waterman-Storer and Salmon, 1998), they are unlikely to account for all of the observed variations in ER morphology. Indeed, ER membrane stacking is readily experimentally inducible without perturbation of the MT cytoskeleton. High level expression of several distinct ER membrane anchored proteins including HMG-CoA reductase (Chin *et al*., 1982), microsomal aldehyde dehydrogenase (Yamamoto *et al*., 1996), cytochrome $b_5$ (Pedrazzini *et al*., 2000), the inositol 1,4,5-triphosphate receptor (Takei *et al*., 1994), and the ER-anchored VAP-B along with its binding partner Nir2 (Amarilio *et al*., 2005) have each been shown to drive ER stacking. In many if not all cases, membrane stacking seems to be driven by the ability of the cytoplasmic domain of the overexpressed protein to interact with itself in-trans, in effect "zippering" apposing membranes together. Even low affinity (100 $\mu$M) interactions between membrane-anchored GFP monomers were sufficient to drive formation of stacked structures as long as the monomers were expressed at high enough concentrations to drive the head-to-head binding reaction (Snapp *et al*., 2003). Thus, it seems that the ER network has an inherent propensity to undergo stacking. As such, a general mechanism for preventing undesired stacking reactions might contribute significantly to the morphogenesis of a dispersed ER network. Conversely, down-regulation of a factor such as Yip1A that promotes network dispersal might provide a mechanism for generating stacked and whorled membranes in accordance with a physiological need, for example, to transiently slow the export of lipid and protein from the ER.

### *Network Dispersal by Yip1A May Involve DP1*

Although transinteractions between ER membrane proteins may underlie ER stacking and whorled ER formation in Yip1A knockdown cells, alternate mechanisms can be envisioned. In this regard, several putative Yip1 binding partners have been reported in yeast (Calero *et al*., 2001; Heidtman *et al*., 2003; Chen *et al*., 2004; Heidtman *et al*., 2005). Among the group, the conserved integral ER membrane protein Yop1 (DP1 in mammalian cells) is unique in its steady-state localization to the ER as well as its previously proposed role in tubulating ER membranes (Voeltz *et al*., 2006). Moreover, an antagonistic relationship between Yip1 and Yop1 has been established in yeast (Calero *et al*., 2001). As such, DP1 stands out as a possible mediator of Yip1A function in ER network dispersal. Indeed, we have observed that both DP1 and the related DP1L1 protein can be coimmunoprecipitated with mammalian Yip1A. Furthermore, DP1 is present in ER membrane whorls (Supplemental Figure 9). However, assessing the functional significance of the interaction will require mapping the DP1 binding determinant in Yip1A and testing whether the binding interaction is required for the network dispersal function of Yip1A. If indeed the ER dispersal function of Yip1A were to involve DP1, it would be of interest to determine whether the underlying mechanism of network dispersal involves the proposed membrane curvature-inducing activity of DP1 (Voeltz *et al*., 2006; Hu *et al*., 2008). For example, Yip1A might be envisioned to negatively regulate DP1, perhaps through competitive inhibition of the homo-oligomerization of DP1 that has been suggested to tubulate ER membranes. In the absence of Yip1A, excessive oligomer-

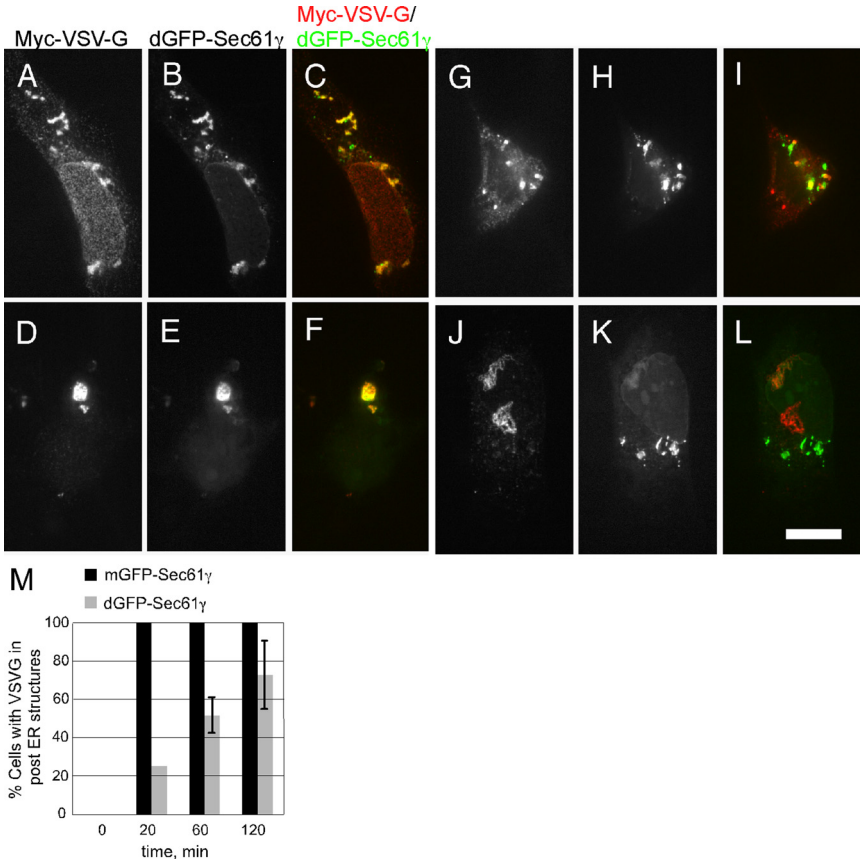


**Figure 9.** ER membrane stacking is sufficient to slow ER export. Cells cotransfected with Myc-ts045 VSV-G and either a control mGFP-Sec61γ construct (not shown but quantified in M) or the ER stack-inducing dGFP-Sec61γ construct were shifted to 40°C to accumulate VSV-G in the ER. Thereafter, cells were shifted to 32°C for 0 (A–C), 20 (D–F), 60 (G–I), or 120 (J–L) min. At the indicated times, cells were fixed and stained with Myc epitope antibodies. The corresponding VSV-G (A, D, G, and J) and GFP-Sec61γ (B, E, H, and K) as well as merged images (C, F, I, and L) are shown. Bar, 10 μm. (M) Quantitation of the kinetics of VSV-G export under each condition, the average of two independent experiments, ±SD is shown.

ization of DP1 would lead to excessive tubulation of the ER, resulting in ER whorls.

### *Additional Roles for Yip1A*

Although our results indicate a novel role for Yip1A in ER membrane morphogenesis, Yip1A may play additional roles in the early secretory pathway. Indeed, although a significant pool of Yip1 is in the ER at steady state (Lorente-Rodriguez *et al.*, 2009), it also seems to cycle rapidly between the ER and Golgi (Heidtman *et al.*, 2003; Yoshida *et al.*, 2008). Therefore, Yip1A seems to exit the ER at a significant rate and may travel as far as the early Golgi before being retrieved back to the ER. Interestingly, Yip1A knockdown has been reported to lead to a reduction in membrane-associated Rab6, suggesting that Yip1A somehow stabilizes Rab6 on membranes (Kano *et al.*, 2009). The loss of membrane-bound Rab6 in turn was associated with a slowing of Shiga toxin trafficking from the Golgi to the ER, suggesting a possible role for Yip1A in Rab6-mediated retrograde trafficking (Sun *et al.*, 2007; Kano *et al.*, 2009). Consistent perhaps with those observations, we have detected a delay in the retrograde redistribution of ERGIC-53 to the ER upon ER export blockade in Yip1A knockdown cells (unpublished data). Thus there may be an additional role for Yip1A in ERGIC-to-ER retrograde transport that might help to explain the Golgi fragmentation observed in Yip1A knockdown cells. Indeed, additional roles for the protein as it cycles through post-ER compartments may account for the ability of Yip1A to interact with specific proteins within the early Golgi. Further work is required to elucidate these other potential roles of Yip1A. Nonetheless, it is important to note that the ER structuring defects observed herein are unlikely to occur as a consequence of Rab6 membrane dissociation or a block in retrograde transport, because previous studies have shown that targeted Rab6 (Sun *et al.*, 2007) and COPI (Guo *et al.*, 2008) knockdown has no obvious effect on ER network morphology.

### *ER Whorling Is Reversible and Regulated*

Concentrically whorled and stacked ER membranes have been documented in a surprising number and variety of normal tissues, although the functional significance of the membrane whorls remains largely unknown (Carr and Carr, 1962; Nickerson and Curtis, 1969; King *et al.*, 1974). Intriguingly, the majority of the tissues in which ER whorls have been documented serve to secrete either peptide or steroid hormones (King *et al.*, 1974). In GnRH-secreting hypothalamic arcuate neurons, ER whorls peak during the diestrus phase of the estrous cycle, diminishing during the proestrus, when an increase in GnRH secretion signals the pituitary to release leutinizing hormone (King *et al.*, 1974). Thus, ER whorling is a reversible process that is regulated by specific signaling pathways. It is tempting to speculate that rearrangement of the ER into whorls may serve to reversibly regulate hormone secretion. Finally, whether the Yip1A-dependent ER dispersal/ER whorling pathway might provide a regulatory mechanism contributing to the formation of such structures is an intriguing possibility that remains to be explored.

## ACKNOWLEDGMENTS

We thank Dr. E. Snapp for the kind contribution of GFP-Sec61γ constructs, members of the Lee and Linstedt laboratories for fruitful discussions, and Drs.

M. Puthenveedu and A. Linstedt for helpful comments on the manuscript. This work was supported by a American Cancer Society Research Scholar grant RGS-07-041-01.

## REFERENCES

Ahluwalia, N., Bergeron, J. J., Wada, I., Degen, E., and Williams, D. B. (1992). The p88 molecular chaperone is identical to the endoplasmic reticulum membrane protein, calnexin. J. Biol. Chem. *267*, 10914–10918.

Amarilio, R., Ramachandran, S., Sabanay, H., and Lev, S. (2005). Differential regulation of endoplasmic reticulum structure through VAP-Nir protein interaction. J. Biol. Chem. *280*, 5934–5944.

Anderson, R. G., Orci, L., Brown, M. S., Garcia-Segura, L. M., and Goldstein, J. L. (1983). Ultrastructural analysis of crystalloid endoplasmic reticulum in UT-1 cells and its disappearance in response to cholesterol. J. Cell Sci. *63*, 1–20.

Aridor, M., and Balch, W. E. (2000). Kinase signaling initiates coat complex II (COPII) recruitment and export from the mammalian endoplasmic reticulum. J. Biol. Chem. *275*, 35673–35676.

Barr, F. A., Puype, M., Vandekerckhove, J., and Warren, G. (1997). GRASP65, a protein involved in the stacking of Golgi cisternae. Cell *91*, 253–262.

Baumann, O., and Walz, B. (2001). Endoplasmic reticulum of animal cells and its organization into structural and functional domains. Int. Rev. Cytol. *205*, 149–214.

Bernales, S., McDonald, K. L., and Walter, P. (2006). Autophagy counterbalances endoplasmic reticulum expansion during the unfolded protein response. PLoS Biol. *4*, e423.

Borgese, N., Francolini, M., and Snapp, E. (2006). Endoplasmic reticulum architecture: structures in flux. Curr. Opin. Cell Biol. *18*, 358–364.

Calero, M., Whittaker, G. R., and Collins, R. N. (2001). Yop1p, the yeast homolog of the polyposis locus protein 1, interacts with Yip1p and negatively regulates cell growth. J. Biol. Chem. *276*, 12100–12112.

Carr, I., and Carr, J. (1962). Membranous whorls in the testicular interstitial cell. Anat. Rec. *144*, 143–147.

Chen, C. Z., Calero, M., DeRegis, C. J., Heidtman, M., Barlowe, C., and Collins, R. N. (2004). Genetic analysis of yeast Yip1p function reveals a requirement for Golgi-localized rab proteins and rab-guanine nucleotide dissociation inhibitor. Genetics *168*, 1827–1841.

Chin, D. J., Luskey, K. L., Anderson, R. G., Faust, J. R., Goldstein, J. L., and Brown, M. S. (1982). Appearance of crystalloid endoplasmic reticulum in compactin-resistant Chinese hamster cells with a 500-fold increase in 3-hydroxy-3-methylglutaryl-coenzyme A reductase. Proc. Natl. Acad. Sci. USA *79*, 1185–1189.

Christensen, A. K., and Fawcett, D. W. (1966). The fine structure of testicular interstitial cells in mice. Am. J. Anat. *118*, 551–571.

Dubois, P., and Girod, C. (1971). Concentric lamellar formations in anterior pituitary cells of the golden hamster. Z. Zellforsch. Mikrosk. Anat. *115*, 196–211.

Feinstein, T. N., and Linstedt, A. D. (2008). GRASP55 regulates Golgi ribbon formation. Mol. Biol. Cell *19*, 2696–2707.

Guo, Y., Punj, V., Sengupta, D., and Linstedt, A. D. (2008). Coat-tether interaction in Golgi organization. Mol. Biol. Cell *19*, 2830–2843.

Heidtman, M., Chen, C. Z., Collins, R. N., and Barlowe, C. (2003). A role for Yip1p in COPII vesicle biogenesis. J. Cell Biol. *163*, 57–69.

Heidtman, M., Chen, C. Z., Collins, R. N., and Barlowe, C. (2005). Yos1p is a novel subunit of the Yip1p-Yif1p complex and is required for transport between the endoplasmic reticulum and the Golgi complex. Mol. Biol. Cell *16*, 1673–1683.

Hu, F. (1971). Ultrastructural changes in the cell cycle of cultured melanoma cells. Anat. Rec. *170*, 41–55.

Hu, J., Shibata, Y., Voss, C., Shemesh, T., Li, Z., Coughlin, M., Kozlov, M. M., Rapoport, T. A., and Prinz, W. A. (2008). Membrane proteins of the endoplasmic reticulum induce high-curvature tubules. Science *319*, 1247–1250.

Hwang, K. M., Yang, L. C., Carrico, C. K., Schulz, R. A., Schenkman, J. B., and Sartorelli, A. C. (1974). Production of membrane whorls in rat liver by some inhibitors of protein synthesis. J. Cell Biol. *62*, 20–31.

Jones, A. L., and Fawcett, D. W. (1966). Hypertrophy of the agranular endoplasmic reticulum in hamster liver induced by phenobarbital (with a review on the functions of this organelle in liver). J. Histochem. Cytochem. *14*, 215–232.

Kabeya, Y., Mizushima, N., Ueno, T., Yamamoto, A., Kirisako, T., Noda, T., Kominami, E., Ohsumi, Y., and Yoshimori, T. (2000). LC3, a mammalian homologue of yeast Apg8p, is localized in autophagosome membranes after processing. EMBO J. *19*, 5720–5728.

Kano, F., Yamauchi, S., Yoshida, Y., Watanabe-Takahashi, M., Nishikawa, K., Nakamura, N., and Murata, M. (2009). Yip1A regulates the COPI-independent retrograde transport from the Golgi complex to the ER. J. Cell Sci. *122*, 2218–2227.

Kapetanovich, L., Baughman, C., and Lee, T. H. (2005). Nm23H2 facilitates Coat Protein II assembly and endoplasmic reticulum export in mammalian cells. Mol. Biol. Cell *16*, 835–848.

King, J. C., Williams, T. H., and Gerall, A. A. (1974). Transformations of hypothalamic arcuate neurons. I. Changes associated with stages of the estrous cycle. Cell Tissue Res. *153*, 497–515.

Koning, A. J., Roberts, C. J., and Wright, R. L. (1996). Different subcellular localization of *Saccharomyces cerevisiae* HMG-CoA reductase isozymes at elevated levels corresponds to distinct endoplasmic reticulum membrane proliferations. Mol. Biol. Cell *7*, 769–789.

Kreis, T. E., and Lodish, H. F. (1986). Oligomerization is essential for transport of vesicular stomatitis viral glycoprotein to the cell surface. Cell *46*, 929–937.

Kuge, O., Dascher, C., Orci, L., Rowe, T., Amherdt, M., Plutner, H., Ravazzola, M., Tanigawa, G., Rothman, J. E., and Balch, W. E. (1994). Sar1 promotes vesicle budding from the endoplasmic reticulum but not Golgi compartments. J. Cell Biol. *125*, 51–65.

Lee, T. H., and Linstedt, A. D. (2000). Potential role for protein kinases in regulation of bidirectional endoplasmic reticulum-to-Golgi transport revealed by protein kinase inhibitor H89. Mol. Biol. Cell *11*, 2577–2590.

Lorente-Rodriguez, A., Heidtman, M., and Barlowe, C. (2009). Multicopy suppressor analysis of thermosensitive YIP1 alleles implicates GOT1 in transport from the ER. J. Cell Sci. *122*, 1540–1550.

Matern, H., Yang, X., Andrulis, E., Sternglanz, R., Trepte, H. H., and Gallwitz, D. (2000). A novel Golgi membrane protein is part of a GTPase-binding protein complex involved in vesicle targeting. EMBO J. *19*, 4485–4492.

Mazzarella, R. A., Srinivasan, M., Haugejorden, S. M., and Green, M. (1990). ERp72, an abundant luminal endoplasmic reticulum protein, contains three copies of the active site sequences of protein disulfide isomerase. J. Biol. Chem. *265*, 1094–1101.

Munro, S., and Pelham, H. R. (1986). An Hsp70-like protein in the ER: identity with the 78 kd glucose-regulated protein and immunoglobulin heavy chain binding protein. Cell *46*, 291–300.

Nakano, A., and Muramatsu, M. (1989). A novel GTP-binding protein, Sar1p, is involved in transport from the endoplasmic reticulum to the Golgi apparatus. J. Cell Biol. *109*, 2677–2691.

Nickerson, P. A., and Curtis, J. C. (1969). Concentric whorls of rough endoplasmic reticulum in adrenocortical cells of the mongolian gerbil. J. Cell Biol. *40*, 859–862.

Ogata, M., *et al.* (2006). Autophagy is activated for cell survival after endoplasmic reticulum stress. Mol. Cell Biol. *26*, 9220–9231.

Pedrazzini, E., Villa, A., Longhi, R., Bulbarelli, A., and Borgese, N. (2000). Mechanism of residence of cytochrome b(5), a tail-anchored protein, in the endoplasmic reticulum. J. Cell Biol. *148*, 899–914.

Presley, J. F., Cole, N. B., Schroer, T. A., Hirschberg, K., Zaal, K. J., and Lippincott-Schwartz, J. (1997). ER-to-Golgi transport visualized in living cells. Nature *389*, 81–85.

Puthenveedu, M. A., and Linstedt, A. D. (2004). Gene replacement reveals that p115/SNARE interactions are essential for Golgi biogenesis. Proc. Natl. Acad. Sci. USA *101*, 1253–1256.

Rajasekaran, A. K., Morimoto, T., Hanzel, D. K., Rodriguez-Boulan, E., and Kreibich, G. (1993). Structural reorganization of the rough endoplasmic reticulum without size expansion accounts for dexamethasone-induced secretory activity in AR42J cells. J. Cell Sci. *105*, 333–345.

Ron, D., and Walter, P. (2007). Signal integration in the endoplasmic reticulum unfolded protein response. Nat. Rev. Mol. Cell Biol. *8*, 519–529.

Rossi, D., Barone, V., Giacomello, E., Cusimano, V., and Sorrentino, V. (2008). The sarcoplasmic reticulum: an organized patchwork of specialized domains. Traffic *9*, 1044–1049.

Sengupta, D., Truschel, S., Bachert, C., and Linstedt, A. D. (2009). Organelle tethering by a homotypic PDZ interaction underlies formation of the Golgi membrane network. J. Cell Biol. *186*, 41–55.

Shibata, Y., Voeltz, G. K., and Rapoport, T. A. (2006). Rough sheets and smooth tubules. Cell *126*, 435–439.

Singer, I. I., Scott, S., Kazazis, D. M., and Huff, J. W. (1988). Lovastatin, an inhibitor of cholesterol synthesis, induces hydroxymethylglutaryl-coenzyme

A reductase directly on membranes of expanded smooth endoplasmic reticulum in rat hepatocytes. Proc. Natl. Acad. Sci. USA *85*, 5264–5268.

Snapp, E. L., Hegde, R. S., Francolini, M., Lombardo, F., Colombo, S., Pedrazzini, E., Borgese, N., and Lippincott-Schwartz, J. (2003). Formation of stacked ER cisternae by low affinity protein interactions. J. Cell Biol. *163*, 257–269.

Soussan, L., Burakov, D., Daniels, M. P., Toister-Achituv, M., Porat, A., Yarden, Y., and Elazar, Z. (1999). ERG30, a VAP-33-related protein, functions in protein transport mediated by COPI vesicles. J. Cell Biol. *146*, 301–311.

Storrie, B., White, J., Rottger, S., Stelzer, E. H., Suganuma, T., and Nilsson, T. (1998). Recycling of Golgi-resident glycosyltransferases through the ER reveals a novel pathway and provides an explanation for nocodazole-induced Golgi scattering. J. Cell Biol. *143*, 1505–1521.

Sun, Y., Shestakova, A., Hunt, L., Sehgal, S., Lupashin, V., and Storrie, B. (2007). Rab6 regulates both ZW10/RINT-1 and conserved oligomeric Golgi complex-dependent Golgi trafficking and homeostasis. Mol. Biol. Cell *18*, 4129–4142.

Takei, K., Mignery, G. A., Mugnaini, E., Sudhof, T. C., and De Camilli, P. (1994). Inositol 1,4,5-trisphosphate receptor causes formation of ER cisternal stacks in transfected fibroblasts and in cerebellar Purkinje cells. Neuron *12*, 327–342.

Tang, B. L., Ong, Y. S., Huang, B., Wei, S., Wong, E. T., Qi, R., Horstmann, H., and Hong, W. (2001). A membrane protein enriched in endoplasmic reticulum exit sites interacts with COPII. J. Biol. Chem. *276*, 40008–40017.

Terasaki, M., Chen, L. B., and Fujiwara, K. (1986). Microtubules and the endoplasmic reticulum are highly interdependent structures. J. Cell Biol. *103*, 1557–1568.

Voeltz, G. K., Prinz, W. A., Shibata, Y., Rist, J. M., and Rapoport, T. A. (2006). A class of membrane proteins shaping the tubular endoplasmic reticulum. Cell *124*, 573–586.

Voeltz, G. K., Rolls, M. M., and Rapoport, T. A. (2002). Structural organization of the endoplasmic reticulum. EMBO Rep. *3*, 944–950.

Waterman-Storer, C. M., and Salmon, E. D. (1998). Endoplasmic reticulum membrane tubules are distributed by microtubules in living cells using three distinct mechanisms. Curr. Biol. *8*, 798–806.

Wiest, D. L., Burkhardt, J. K., Hester, S., Hortsch, M., Meyer, D. I., and Argon, Y. (1990). Membrane biogenesis during B cell differentiation: most endoplasmic reticulum proteins are expressed coordinately. J. Cell Biol. *110*, 1501–1511.

Yadav, S., Puri, S., and Linstedt, A. D. (2009). A primary role for Golgi positioning in directed secretion, cell polarity, and wound healing. Mol. Biol. Cell *20*, 1728–1736.

Yamamoto, A., Masaki, R., and Tashiro, Y. (1996). Formation of crystalloid endoplasmic reticulum in COS cells upon overexpression of microsomal aldehyde dehydrogenase by cDNA transfection. J. Cell Sci. *109*, 1727–1738.

Yoshida, Y., *et al*. (2008). YIPF5 and YIF1A recycle between the ER and the Golgi apparatus and are involved in the maintenance of the Golgi structure. Exp. Cell Res. *314*, 3427–3443.